Analyst

Accepted Manuscript

ROYAL SOCIETY OF CHEMISTRY

www.rsc.org/analyst

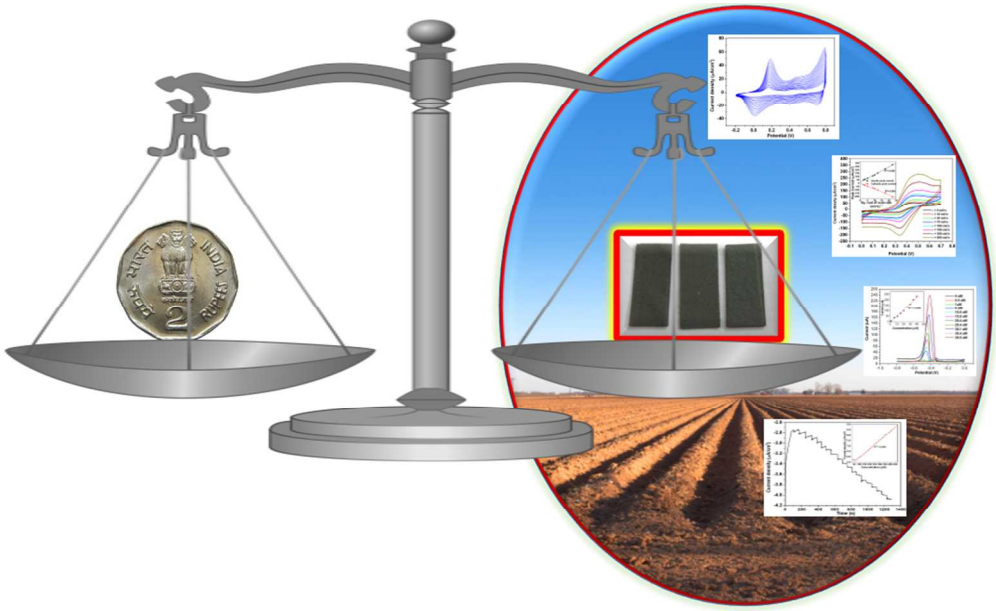

284x172mm (96 x 96 DPI)

Analyst

RSCPublishing

ARTICLE

Polymer-graphite composite: A versatile use & throw plastic chip electrode

Cite this: DOI: 10.1039/x0xx00000x

Mosarrat Perween[a,b], Dilip B. Parmar[a] ,Gopala Ram Bhadu[a] and Divesh N. Srivastava[a,b*].

Received ooth January 2012,
Accepted ooth January 2012

DOI: 10.1039/x0xx00000x

www.rsc.org/

We report an efficient plastic chip electrode (PCE) fabricated from the composite of graphite and poly (methyl methacrylate) by simple solution casting method and promoted as economically cheap multipurpose disposable electrodes for various applications. The TEM images of the filler (graphite) show that the material consists of single as well as multilayers. The self-standing and arid electrodes thus prepared were characterized for their material properties like, microscopy (SEM and AFM), thermal properties (TGA), mechanical (tensile strength) and electrical properties. A set of physical parameters were derived from these characterizations for sustainability of these electrodes in harsh off-laboratory conditions. The utility of these mechanically stable, bulk conducting and high surface area electrodes were demonstrated in various well understood electrochemical protocols, like cyclic voltammetry, stripping voltammetry, electropolymerization, electrowinning and amperometric sensing. The voltammetry data were compared with the data recorded on conventional glassy carbon electrode.

Introduction

Use of carbon as electrode material dates back to the mid of the last century[1] when wax[2] and epoxy[3] impregnated graphite solid electrodes were tried in polarography. They were considered 'unconventional' then, as they were the first solid electrodes, apart from precious metals like platinum and gold, after Heyrovsky's liquid Dropping Mercury Electrode (DME). The advantageous attributes of the solid carbon electrodes over the traditional electrodes of those days included low background current, large potential window and ease of modification. Nonetheless, with time those unconventional electrodes became more and more obvious and glassy carbon electrode is one of the extensively used working electrode these days along with platinum and gold. In spite graphite continued to be a wonder constituent of tailored electrodes. After the first report of carbon electrode several attempts were made towards further tailoring of these electrodes, though the choice of graphite powder and paraffin oil for making carbon paste continued for several years monotonically[4]. The early attempts with such composite had preferred the traditional (pencil like) electrode arrangements[5]. In recent era more robust composites comprising graphite/ graphene in polymer matrix and commercially available binders (Nujol, Uvasol) are reported[6, 7]. Similarly, newer techniques like screen-printing[8-10], sputtering[11] and conducting coating[12] started emerging for tailoring of the electrodes.

The screen-printing technology is ideal for production of disposable tailored electrodes as its fabrication does not require any complicated or expensive equipment and the process is simple, rapid and easy to automate. In addition to carbon based printing inks several other materials such as gold[13, 14], platinum[15], silver[16] are also used. These tailored electrodes have several leads over the conventional carbon electrodes. Lower oxidation potential compared to the traditional carbon and platinum electrode has been reported on the surface of the screen-printed carbon electrode[17]. Wang compared the electrochemical and electrokinetic behavior of various screen-printed electrodes fabricated in different conditions[18]. Additionally, the printing ink has been used as immobilization matrix for the receptors and biomolecules[19, 20]. Moreover, being cost effective these electrodes are ideal for one-time use applications. There are several reviews available in literature discussing various aspects along with applications of the screen-printed electrodes[21, 22].

Although, the screen-printed electrodes due to its flat and sleek two dimensional geometry fits well for the field, on-site as well as more advanced applications like interdigitated array electrodes[23-25] and lab-on-a-chip[26]. Still the bottleneck with coated and screen-printed electrodes is that the conducting layers are not the integral part of the base/ substrate on which electrode is fabricated and can easily get delaminated due to mechanical jerk or high current[27] . Therefore, there was a need for an improved alternative of the surface coated electrodes having similar potentials but minimized shortcomings. In current article

we report a different approach of fabricating flat and self-standing two dimensional electrode using bulk conducting polymer composite. The amount of conducting filler (graphite) was maintained above the earlier reported percolation threshold for the two dimensional systems on the basis of theoretical[28] as well as experimental[29-31] considerations. Although this type of electrode material is known in the literature[31, 32], but its comprehensive application as electrode in electroanalyses are not available to the best of our information. Albeit their application in battery[33A], double-layer capacitor[34B] and fuel cell[35C] is known. Further, this method eliminates the thermal curing steps also, which is an essential step in fabrication of screen-printed electrode[36] and can be considered as an added advantage of PCE in biosensing applications. The composite was solution casted and cut in to small chips to use as working electrode in conventional three electrode electrochemical cell.

Experimental

Materials

The graphite powder (CDH Pvt. Ltd.), Poly (methyl methacylate) (Otto kemi Pvt. Ltd.) were used without any further purification or pretreatment. Anhydrous sodium acetate, acetic acid, potassium hydrogen phthalate used for buffer preparation were purchased from Sigma Aldrich. Potassium ferrocyanide, ferrocenecarboxylic acid, potassium nitrate, potassium chloride and hydrogen peroxide (30 % v/v) were purchased from Spectrochem Pvt. Ltd. (India) while lead nitrate, zinc sulphate, manganese sulphate, iron (II) sulphate were obtain from CDH Pvt. Ltd. Aniline received from Sigma Aldrich and used after double distillation. All chemicals and solvent (chloroform) used were of analytical grade. High quality polyester sheets employed as template in composite preparation were purchased from local vendor.

Preparation of plastic chip electrode

PCEs were fabricated using graphite and Poly (methyl methacrylate) (PMMA) in 60:40 ratio. A viscous suspension was prepared by dispersing graphite (3.6 g) in polymer (2.4 g) solution in chloroform (25 mL). A glass mould (10 × 10 cm) was prepared for solution casting of the composite. The pictorial representation for making the electrode is given in Figure S-1 (supplementary information). A polyester sheet was spread in the bottom of the mould keeping its edges above the walls of the glass mould (Fig. S-1A). The graphite-PMMA slurry was spread over this polyester sheet (Fig. S-1B & C) and dried at room temperature (Fig. S-1D). A typical thickness of the sheet under the above mentioned conditions was found around 0.45 mm. The sheet was cut into pieces of appropriate dimension for various characterizations and in 0.8 cm x 3 cm dimension (Fig. S-1H) for using as working electrode in various electrochemical applications, maintaining the working length 0.5 cm by protecting remaining portion by .teflon tape except the contacts.

Characterization of plastic chip electrode

Characterization of the PCE has been carried out to understand it's physical properties. On the basis of these fundamental properties a set of parameters were derived for successful use of these electrodes in off-laboratory conditions. The Transmission Electron Microscopy (TEM) (JEOL, JEM 2100) of the graphite was carried out before using it in composite. Approximately10 mg graphite powder was dispersed in 1 mL chloroform and loaded over a lacey carbon coated copper grid (300 mess) and solvent was evaporated under ambient conditions followed by the images were recorded at 200 kV acceleration voltage. The surface morphology of the PCE was investigated by Scanning Electron Microscope (SEM) (LEO 1430VP) after thin coating of conducting Au-Pd alloy and Atomic Force Microscope (AFM) (NT-MDT Ntegra Aura) without any pre-treatment over 0.8 × 2 cm sized sample. Tensile tests were carried out using universal testing machine (Zwick Roell, type X force P, S/N 756324) applying a preload of 0.01 N at a speed of 0.2 mm/min. Young's modulus was determined from the regression slop in the elastic region of the stress strain curve. The specimen dimensions for tensile test was 8× 0.45 ×35 mm (w × t × l). The test was repeated four times to get a mean value. The thermal stability of the chip electrode was examined through thermogravimetric analysis (TGA) (NETZSCH, TG 209 F1, libra) taking 30 mg of sample. The measurements were performed from 25°C to 600°C with a heating rate of 10°C/min in continuous flowing nitrogen atmosphere (50 mL/min). The first derivative of the TGA data was taken to get Differential thermal analysis (DTA) curve. The current-voltage (I-V) characteristic of the chip electrode was investigated by measuring current in ± 100 mV bias voltage window using Source Meter Unit (Keithley 2635A). The measurements were performed using a strip of 1 cm × 1cm dimension sandwiched between two platinum foils (ohmic contacts) in the maxilla of a spring loaded brass holder.

Electrochemical measurements

The performance of PCE was evaluated on the basis of various standard and well understood electrochemical protocols. Experiments were performed using potentiostat (Princeton applied research PARSTAT 2273) and bipotentiostat (PINE AFCBP1) in a 10 mL open glass cell at room temperature (24 ± 2°C). A three electrode assembly was used in all measurements in which PCEs were employed as working electrode connected through the crocodile clip, while an Ag/AgCl (sat KCl) and platinum foil were used as reference and auxiliary electrodes respectively. All aqueous solutions were prepared using Milli Q water (resistivity ≥ 18 M Ω). 0.1M acetate buffer of pH 4.5 were used as electrolyte for the preparation of Tris(2,2′-bipyridyl)dichlororuthenium(II) hexahydrate (1mM) and potassium ferrocyanide (10mM) solutions while 3mM ferrocene carboxylic acid solution was made in 0.1 M potassium nitrate. Cyclic voltammograms were recorded at different scan rate for all the above redox couple. For ASV, a stock solution (1mM) of lead nitrate was prepared in acetate buffer (0.1M) of 4.5 pH. Various concentrations of lead ranging from 0.5 μM to 40 μM were prepared by successive dilution of stock solution with same buffer. Lead was deposited on the PCE at -1.2V for 5 minutes with continuous stirring. . The voltammogram was recorded after 5 seconds equilibration by applying differential pulse voltammetry; under following parameters- potential range -0.8 V to 0 V, pulse width 25mV for 50msec, step height 2mV and step time 100 msec. Electrochemical polymerization was tried on PCE using freshly prepared aniline sulphate monomer, which was prepared by dissolving 0.1 M of aniline in 0.5 M H_2SO_4 acid. The electropolymerization was carried out by potentiodynamic method (potential range -0.2 V to 0.8 V) for 35 cycles.

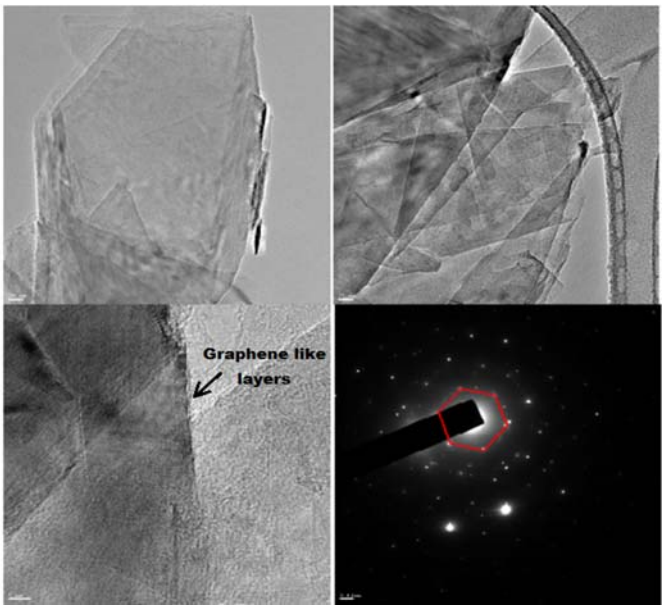

Figure 1. Transmission electron micrograph of the filler graphite depicting (A) single graphene like sheet; (B) multilayer sheets; (C) transverse view of layered stacks; (D) selected area electron diffraction (SAED) pattern of 1A.

Galvanostatic electrowinning of zinc was tried on the PCEs using synthetic solution having same composition as present in neutral kidd creek zinc electrolyte[37] [i.e. zinc 167.5 g/L, manganese 5.5 g/L, and iron 7 g/L]. Three different current densities viz. 0.25, 1.25 and 2.25 mA/cm^2 were examined for the zinc deposition. Finally, these PCEs were utilized in amperometric sensing of hydrogen peroxide. For this purpose, 1 mM H_2O_2 stock solution was prepared in 0.1 M phosphate buffer (pH 5.2). The sensor responses were recorded at -0.2 V potential after attaining the steady state by successive addition of 100 µL of stock solution under stirring condition.

Results and discussion

Characterization of the filler

Since, the percolation threshold of a composite is highly dependent on the structure of the filler, therefore, the structural characterization of the filler (graphite) was carried out before using it in the PCE. The TEM images of the filler are given in the Figure 1. From the TEM images it is clear that the filler consist of single (Figure 1A) as well as a few layered (Figure 1B) graphene like sheets. The average size of the sheets were found to be varying within the range of few micro meters, whereas the interplanar distance were found to be 3.33 Å as measured from the profilogram recorded from the layered stacks (Figure S-2, in supporting information). The selected area electron diffraction (SAED) pattern recorded from the graphite layers is given in the Figure 1D. The high crystallinity of the material is clearly demonstrated by the diffraction pattern. The characteristic diffraction spots related to the hexagonal symmetry of graphite is also clearly visible in the diffraction pattern. These thin sheets of graphite form the continuous percolating path through the polymer matrix for smooth transfer of the charge carrier.

Characterization of plastic chip electrode

Microstructure: The surface topography of the PCE was studied by Scanning Electron Microscopy (SEM) and Atomic Force Microscopy (AFM). The SEM image of the chip electrode surface is given in Figure 2. Highly rough morphology of the surface can be seen in the figure with bulging of few tens of nanometers (region 'A' in Figure 2), interrupted with few micron sized islands (region 'B' in Figure 2). These rough morphologies are due to the random orientation of the graphite particles in the polymer matrix and are responsible for giving high surface area to the electrode. These surface roughnesses are better realized in the AFM images. The 3D AFM image of region 'A' is given in Figure 3A. The graphite particles peeping from the polymer matrix can be seen. The 2D scaffold of the region 'A' is given in the *in-set* of the Figure 3A. The average roughness in region 'A' was found to be 4.77 nm and peak to valley height of 50.21 nm. The 3D AFM image of region 'B' is given in Figure 3B and its corresponding 2D scaffold in the in-set. The observed average roughness in region 'B' was 217.13 nm and peak to valley height 1.76 microns (Figure 3B). The data are summarized in table T-1 in the supporting information along with other physical properties of the PCE.

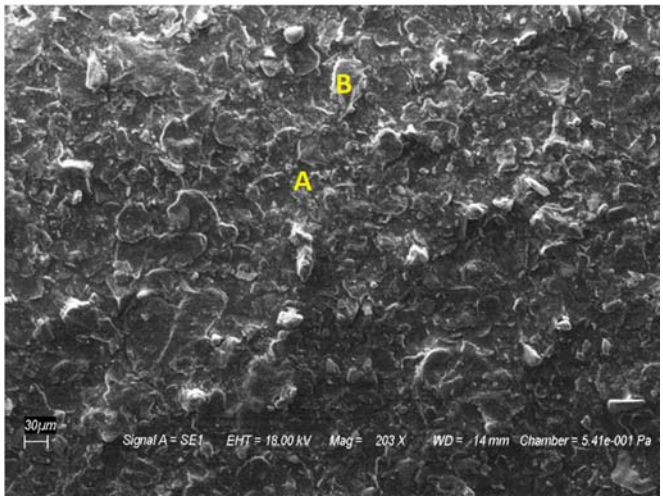

Figure 2. The surface topography of the plastic chip electrode as seen under scanning electron microscope.

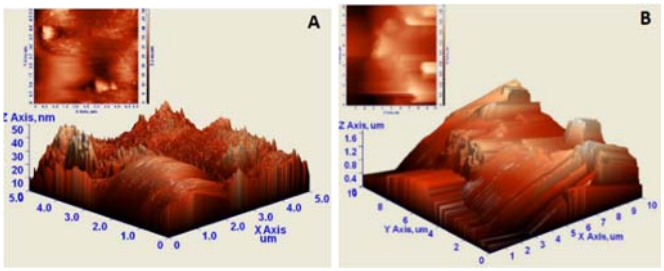

Figure 3. The 3D surface topography of the plastic chip electrode as seen under atomic force microscope; A) region 'A' of Figure 2; B) region 'B' of Figure 2. [In-set: corresponding 2D scaffolds].

Thermal properties: Thermogravimetric (TGA) curve of chip electrode is shown in Figure 4. No significant weight loss was observed till around 130°C, which indicates that the electrode was completely dry. A small decomposition of around 4% was observed at 132°C and attributed to the loss of trapped and bonded solids/solvent. The onset decomposition temperature

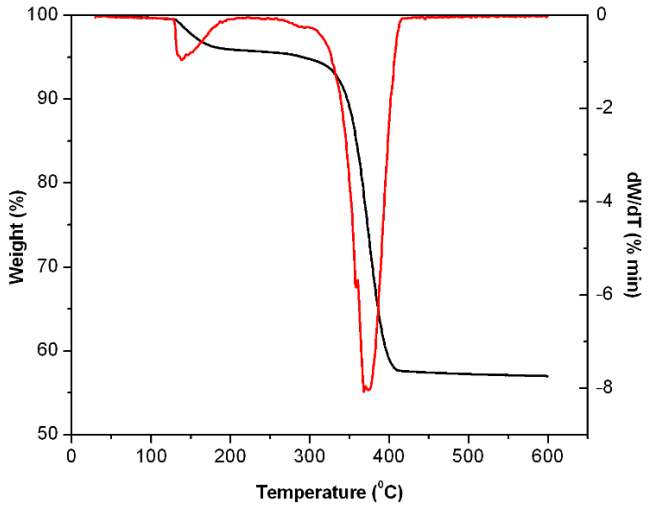

Figure 4. Theromogravametry analysis [black curve on Y axis] and its differential curve (DTA) [red curve on Y' asix] of plastic chip electrode.

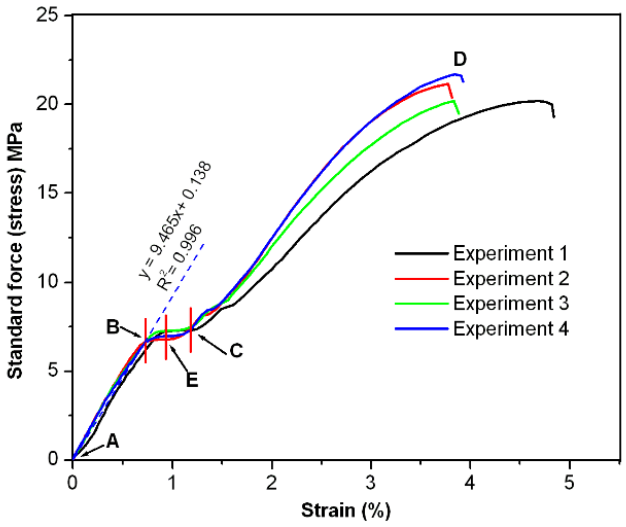

Figure 5. Stress-strain plot of plastic chip electrode.

(temperature at which first 10% weight loss observed)[38] was found around 346°C. A total of 43% weight loss was observed between 346°C to 404°C with maximum weight loss at 368°C as seen from the DTA plot (Figure 4). These results are in accordance with the earlier reports and attributed to the decomposition of main chain of the PMMA[32]. While PMMA begins to degrade at about 285°C[39, 40], with a total weight loss of 95.5%[41], it can be seen from these data that onset decomposition temperature of PCE is about 61°C higher than that of pure PMMA, which indicates higher thermal stability of the electrode. Pure graphite exhibits very high thermal stability with only 1.6% total weight loss up to 800°C[42] , therefore no significant weight loss has been observed till 600°C. The results obtained from the thermal analysis provides an evidence for the expected composition of the composite.

Mechanical properties: The stress-strain curve recorded during the tensile testing is given in the Figure 5. The shape of the stress-strain curve observed in current study is typical for a ductile material[43], consisting of an elastic or proportionality region (section 'AB' in the curve), a distinct elastic limit (point 'E'), yield point (point 'C', where inelastic deformation starts) and a failure point (point 'D', where electrode snaps). Whereas all the four sets of data are superimposable in the elastic region, some deviations have been observed in the inelastic region and the failure point was observed between 4-5% strain. The Young's modulus was calculated from the slope of the elastic region and found to be 0.95 GPa. The neat PMMA has a young's modulus value of 2.1 GPa[39]. The lowering of the Young's modulus in case of PCE is due to the fact that higher amount of filler beyond a certain limit does not reinforces the polymer matrix[42] as it does in case of lower amount of filler[44]. The data of the mechanical characterization of the PCE are tabulated in table T-1 (see supporting information).

Electrical Properties: After thorough characterization of various physical properties of the PCE it was set for the electrical characterization. The bulk conductivity was measured by sandwiching the chip electrode between two platinum electrodes in a spring loaded sample holder. The current-voltage characteristics (I-V) was recorded in ±100 mV bias voltage window and found absolutely linear (R^2 = 1) which indicates ohmic nature of the electrode. The I-V curve is given in Figure S-3. The specific conductance was calculated by normalizing the slope of the curve with dimension of the chip electrode and found to be 19.75 mS/cm, the data is summarized in table T-1 (see supporting information).

Applications of plastic chip electrode

Cyclic voltammetry: Cyclic voltammograms (CVs) were recorded at different scan rate for the three redox couples. Scan rate varied from 5 mV/s to 300 mV/s for ferrocyanide/ fericyanide couple (Figure 7A), 5 mV/s to 500 mV/s for ferrocene/ frrocenium couple (Figure 7B) and 5 mV/s to 200 mV/s for $[Ru(bpy)_3]^{+2}/[Ru(bpy)_3]^{+3}$ couple (Figure 7C). The parameters of the redox peaks are furnished in table T-2 (see supporting information). The ΔE for all the three redox show super nernstian behavior (ΔE larger than 59 mV/s for one electron transfer), which is in accordance with earlier reports for graphite[45]. Moreover, the super nernstian behavior was found increasing for all redox couples as a function of scan rate (table T-2 [supporting information]). Such a high deviation from nernstian behavior suggesting the quasi reversible electron transfer process at higher scan rates[46, 47]. Further, both cathodic and anodic peaks were found broader for all the redox couple, this observation is attributed to the semiconducting nature of the PCE. The peak current values for cathodic as well as anodic peaks were plotted against square root of scan rate (√ν) and are given in the in-set of the corresponding CVs (Figure 7 A-C). It was observed that both the peak currents (Ip) were increasing linearly (R^2 value was higher than 0.995 in all cases) with √ν, suggesting mass transport are predominantly diffusion controlled and PCE is electrochemically inert for the redox species and he solvent in the studied potential window. However, small intercept in the Ip versus √ν plots were observed which can be correlated to the small non-faradaic current generated due to relatively more dielectric nature of the PCE than the conventional noble metal electrodes. The formal potentials (E^0) were calculated by taking mean of cathodic and anodic peak potential and produced in table T-2 (supporting information).

Further, the CVs recorded on PCE were compared with glassy carbon electrode. Such a representative example for ferrocene/ ferrocenium redox couple is given in the Figure S-4 in

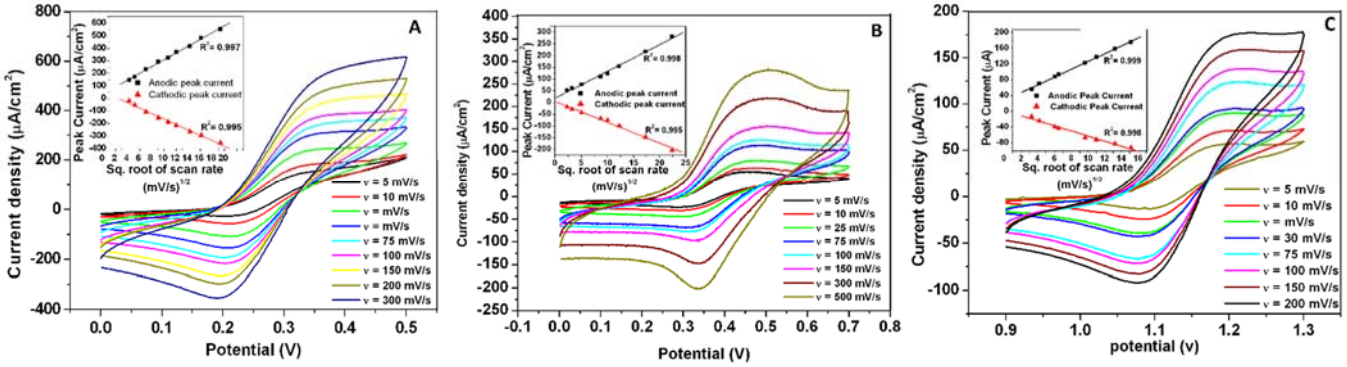

Figure 7. Cyclic voltammogram of A) ferrocyanide/fericyanideredox couple; B) ferrocene/ frroceniumredox couple; C) [Ru(bpy)3]+2/[Ru(bpy)3]+3redox couple recorded on plastic chip electrode. [In-set – Corresponding peak current vs. square root of scan-rate plot for cathodic as well as anodic scans].

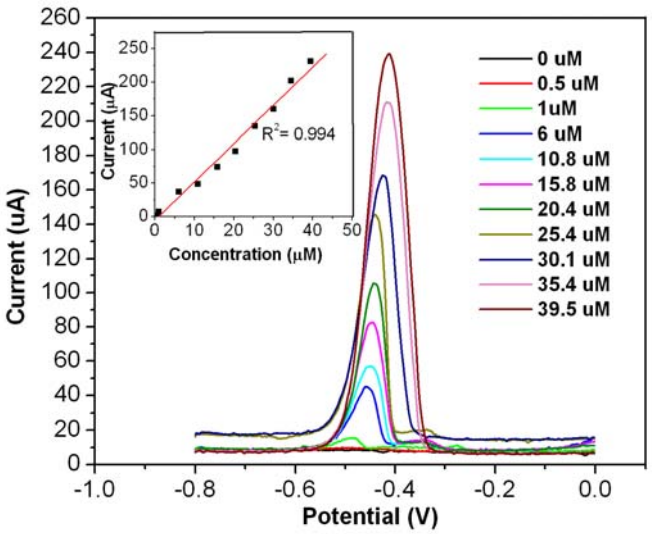

Figure 8. Stripping step of DPASV for Pb+2 on plastic chip electrode at various concentrations of the analyte. [In-set-Corresponding calibration curve].

the supporting information. Almost twice the current density for PCE as compared to conventional glassy carbon electrode can be seen in the plot. This high current is attributed to the high surface area of the PCE as seen in microscopy. The broad peaks are observed in case of PCE compared to conventional glassy carbon electrode is already discussed. A blank scan (cycling in supporting electrolyte without analyte using PCE as working electrode) is also given in Figure S-4. The curve falls on the baseline without any peak indicating very small non-faradaic current, which is in accordance with the Ip versus √ν plots. Similar electrode surface effects have been observed for other redox couples as well.

Stripping voltammetry: Figure 8 illustrates the stripping step of a typical anodic stripping voltammetry for different concentrations of lead ranging from 0.5 μM (0.1 ppm) to 40 μM (8.2 ppm) obtained on PCE using differential pulse technique. Symmetrical, sharp and well-defined striping peaks around -0.45 V were observed. Prior to stripping the lead ion was deposited over the PCE at -1.2 V. The peak current was normalized with the base line current i.e. current at zero concentration of lead. The normalized current was used to draw the calibration curve which is given in the in-set of figure 8 and found to be linear in 1 μM to 40 μM concentration range with a coefficient of regression (R^2) 0.994. The needle shaped crystals of lead deposited on PCE surface, as recorded by SEM, is given in the Figure S-5A. The EDX (Figure S-5B) confirms these crystals as lead.

Electrowinning: It is known that electrodeposition of zinc proceeds through the nucleation and growth mechanism[48]. The formation of nucleus can easily be seen in the SEM image (Figure S-6A & S-6B), taken just after initiation of electrodeposition, which is supported by EDX (Figure S-6C). Cyclic voltammogram Zn^{+2} (figure S-7A) shows hysteresis loop with a crossover which is characteristic of nucleation and growth mechanism[49]. The crossover potential (E_{co}) of Zn^{+2} on PCE was found to be -0.96 V (vs Ag/AgCl (sat KCl)), which is almost same to the E_{co} of Zn^{+2} on various conventional electrodes[50]. Galvanostatic deposition of Zn^{+2} was also tried over PCE at three different current densities. Resulted chronopotentiometric curve is given in Figure S-7B which shows similar behavior as typically shown by nucleation and growth process[51]. Whereas the plot at high current density was found very smooth, a shoulder has been observed at lower current density depositions. This can be explained by the fact that the rate of nucleation is far above than that of growth of nuclei in case of high current density which covers most of the surface and causes faster stabilization of potential while low current density involves in growth of nuclei which delay the surface covering and takes more time for potential stabilization.

Electropolymerization: Anodic oxidation of aniline to synthesize polyaniline (PANI) on PCE was tried using potentiodynamic technique. The cyclic voltammogram of the electropolymerization is given in Figure 9. A typical voltammogram of polyaniline redox consists of two anodic peaks of polymer oxidation one at around +160 mV and other around +800 mV. The first peak corresponds to conversion of leucoemeraldine form of polyaniline to emeraldine form (formation of polaron in acidic medium) whereas the second peak corresponds to conversion of emeraldine form to pernigraniline form (formation of bipolaron). Further, the monomer oxidation peak also appears at +800 mV potential and hence it is difficult to differentiate these superimposed monomer oxidation and bipolaron formation peaks, although their corresponding cathodic peaks can easily be seen in the reverse scan. Another peak is sometimes seen in the CV of polyaniline particularly when the polymer is thick enough. This peak

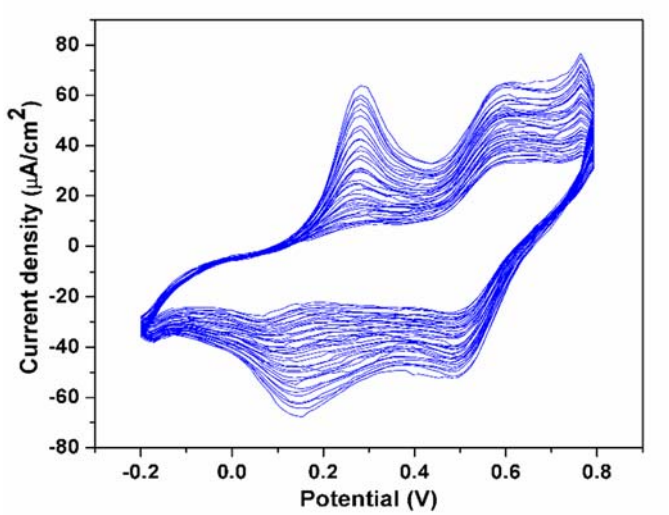

Figure 9. Cyclic voltammogram of electropolymerization of aniline on plastic chip electrode in aniline sulphate monomer having 0.1 M of aniline in 0.5 M H2SO4 acid.

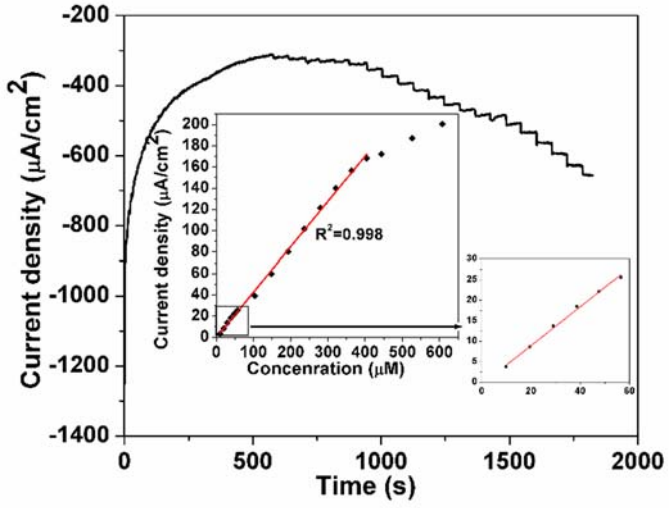

Figure 10. Chronoamperometric response recorded at -0.2 V vs. Ag/AgCl for successive addition of 100 μL of 1 mM H_2O_2. [Inset: calibration curve of limiting current vs. concentration of H_2O_2].

corresponds to overoxidative degradation of polyaniline and appears at around +500 mV potential[52]. Although, some other authors assigned this as due to crosslinking of polyaniline[53, 54]. All these characteristic peaks of polyaniline redox were well resolved on PCE as can be seen in Figure 9.

Amperometric sensing: Chronoamperometric technique has been employed for non-enzymatic amperometric sensing of H_2O_2 on PCE. The initial steady state was achieved after around 550 seconds, following to that the addition of H_2O_2 was started. After addition of each aliquot of H_2O_2 the reduction current increases sharply and then reaches a stable value in less than 10 seconds, indicating quick response of electrode (Figure 10). Successive aliquots of H_2O_2 was added at an interval of 1 minute and steady state current was recorded. The calibration curve was plotted by normalizing the reduction current with the background current (current in absence of H_2O_2) and given in in-set of Figure 10. It can be seen in the calibration curve that the device shows linear behavior (R^2 = 0.998) in wide concentration window (9 μM to 400 μM). The sensitivity, calculated from the slop of calibration plot, is found to be 0.42 μA/μM. The lower detection limit was found to be 9 μM. This value is quite low for an untailored sensor reported earlier[55]. This low detection limit is attributed to the high surface area of PCE.

Conclusions

PCE fabricated from the bulk conducting (σ = 19.7 mS/cm) polymer composite of graphite is reported for off-lab use and throw applications. On the basis of material characterization it was concluded that these electrodes can best used up to 0.8% strain (tensile testing), although the material is thermally stable up to 350°C. The microscopy indicated high surface area of the electrode through surface roughness and manifested by high current in cyclic voltammogram compared to the conventional glassy carbon electrode. The electrode fabricated was found suitable as working electrode in number of electrochemical reaction like cyclic voltammetry, anodic stripping voltammetry, electrowinning, electropolymerization and amperometric sensing. Little underperformance of this electrode in some electroanalysis can be overcome by the further application specific tailoring.

Acknowledgements

The authors are thankful to the Department of Science and Technology (DST), Govt. of India for the financial support in terms of grant-in-ad project (ID/SEN/139/2008) and XII FYP project MULTIFUN (CSC-0101). MP acknowledges the Junior Research Fellowship (JRF) received from the same project.
CSIR-CSMCRI Registration Number: 075/2014.

Notes and references

[a] Analytical Discipline and Centralized Instrument Facility, CSIR - Central Salt & Marine Chemicals Research Institute, Gijubhai Badheka Marg, Bhavnagar - 364 002, India.
[b] Academy of Scientific & Innovative Research, CSIR-CSMCRI, Gijubhai Badheka Marg, Bhavnagar - 364002, India.

Electronic Supplementary Information (ESI) available: [Graph for electrowinning of zinc, I-V Characteristics of PCE, Comparative cyclic voltammogram between PCE and glassy carbon electrode, pictorial representation of electrode making process and several SEM images with EDX spectra are available in Supporting Information.]. See DOI: 10.1039/b000000x/

1. R. N. Adams, *Anal. Chem.* , 1958, **30**, 1576-1576.
2. V. F. Gaylor, A. L. Conrad and J. H. Landerl, *Anal. Chem.* , 1957, **29**, 224-228.
3. H. S. Swofford and R. L. Carman, *Anal. Chem.*, 1966,, **38**, 966-969.
4. I. Švancara, K. Vytřas, J. Barek and J. Zima, *Crit. Rev. Anal. Chem.*, 2001, **31**, 311-345.
5. B. B. Prasad, R. Madhuri, M. P. Tiwari and P. S. Sharma, *Sensor. Actuat. B*, 2010, **146**, 321-330.
6. K. Kalcher, J.-M. Kaufrnann, J. Wang, I. Švancara, K. Vytřas, C. Neuhold and Z. Yang, *Electroanalysis*, 1995, **7**, 5-22.
7. J.-B. He, X.-Q. Lin and J. Pan, *Electroanalysis*, 2005, **17**, 1681-1686.
8. J. E. Frew, S. W. Bayliff, P. N. B. Gibbs and M. J. Green, *Anal. Chim. Acta*, 1989, **224**, 39-46.
9. I. J. Higgins, J. M. McCann, G. Davis, H. A. O. Hill, R. Zwansiger, B. L. Treidl, N. N. Birket and E. V. Plotkin, *Eur. Pat. Appl.*, EP 0127958 A2, 1984.
10. S. A. Wring and J. P. Hart, *Analyst*, 1992, **117**, 1281-1286.

11. A. M. Bond, T. L. E. Henderson and W. Thormann, *J. Phys. Chem.*, 1986, **90**, 2911-2917.
12. Marco-A. De Paoli, Robert J. Waltman, Arturo F. Diaz and J. Bargon, *J. Chem. Soc. Chem. Commun.*, 1984, 1015-1016.
13. R. García-González, M. T. Fernández-Abedul, A. Pernía and A. Costa-García, *Electrochim. Acta*, 2008, **53**, 3242-3249.
14. S. Laschi, I. Palchetti and M. Mascini, *Senor. Actuat. B*, 2006, **114**, 460-465.
15. J. P. Metters, F. Tan, R. O. Kadara and C. E. Banks, *Anal. Methods*, 2012, **4**, 1272-1277.
16. J.-M. Zen, C.-C. Yang and A. S. Kumar, *Anal. Chim. Acta*, 2002, **464**, 229-235.
17. V. Vasjari, A. Merkoci, J. P. Hart and S. Alegret, *Microchim. Acta* 2005, **150**, 233-238.
18. J. Wang, B. Tian, V. B. Nascimento and L. Angnes, *Electrochim. Acta* 1998, **43**, 3459-3465.
19. C. A. Marquette, M. F. Lawrence and L. J. Blum, *Anal. Chem.*, 2006, **78**, 959-964.
20. J. D. Newman, A. P. F. Turner and G. Marrazza, *Anal. Chim. Acta*, 1992, **262**, 13-17.
21. M. Li, Y.-T. Li, D.-W. Li and Y.-T. Long, *Anal. Chim. Acta*, 2012, **734**, 31-44.
22. K. C. Honeychurch and J. P. Hart, *TrAC Trends in Analytical Chemistry*, 2003, **22**, 456-469.
23. D. G. Sanderson and L. B. Anderson, *Anal. Chem.*, 1985, **57**, 2388-2393.
24. H. Tabei, M. Morita, O. Niwa and T. Horiuchi, *J. Electroanal. Chem.*, 1992, **334**, 25-33.
25. Y. Ueno, K. Furukawa, K. Hayashi, M. Takamura, H. Hibino and E. Tamechika, *Anal. Sci.*, 2013, **29**, 55-60.
26. R. Daw and J. Finkelstein, *Nature*, 2006, **442**, 367.
27. J. K. Jeszka, A. Tracz, J. Ulanski and M. Kryszewski, *J. Phys.D: Appl. Phys.*, 1985, **18**, L167.
28. M. F. Sykes and J. W. Essam, *Phys. Rev.*, 1964, **133**, A310-A315.
29. B. J. Last and D. J. Thouless, *Phys. Rev. Lett.*, 1971, **27**, 1719-1721.
30. D. N. Srivastava and R. A. Singh, *Synth. Met.*, 2000, **114**, 361–364.
31. S. Stankovich, D. A. Dikin, G. H. B. Dommett, K. M. Kohlhaas, E. J. Zimney, E. A. Stach, R. D. Piner, S. T. Nguyen and R. S. Ruoff, *Nature*, 2006, **442**, 282-286.
32. X. Zeng, J. Yang and W. Yuan, *Eur. Polym. J.*, 2012, **48**, 1674-1682.
33. S. Komaba, N. Yabuuchi, T. Ozeki, Z.-J. Han, K. Shimomura, H. Yui, Y. Katayama and T. Miura, *J. Phys. Chem. C*, 2011, **116**, 1380-1389.
34. G. Oskam and P. C. Searson, *J. Phys. Chem. B*, 1998, **102**, 2464-2468.
35. R. Kannan, P. P. Aher, T. Palaniselvam, S. Kurungot, U. K. Kharul and V. K. Pillai, *J. Phy. Chem. Lett.*, 2010, **1**, 2109-2113.
36. J. Wang, B. Tian, V. B. Nascimento and L. Angnes, *Electrochim. Acta*, 1998, **43**, 3459-3465.
37. A. M. Alfantazi and D. B. Dreisinger, *J. Appl. Electrochem.* , 2001, **31**, 641-646.
38. M. C. Costache, D. Wang, M. J. Heidecker, E. Manias and C. A. Wilkie, *Polym. Adv. Techno.*, 2006, **17**, 272-280.
39. T. Ramanathan, A. A. Abdala, S. Stankovich, D. A. Dikin, M. Herrera-Alonso, B. D. Piner, D. H. Adamson, H. C. Schniepp, X. Chen, R. S. Ruoff, S. T. Nguyen, I. A. Aksay, R. K. Prud'homme and L. C. Brinson, *Nat. Nanotechnol.*, 2008, **3**, 327-331.
40. T. Ramanathan, S. Stankovich, D. A. Dikin, H. Liu, H. Shen, S. T. Nguyen and L. C. Brinson, *J. Polym. Sci. Polym. Phys.*, 2007, **45**, 2097-2112.
41. L. Ye, X.-Y. Meng, X. Ji, Z.-M. Li and J.-H. Tang, *Polym. Degrad. Stab.*, 2009, **94**, 971-979.
42. A. Yasmin and I. M. Daniel, *Polymer*, 2004, **45**, 8211-8219.
43. J. R. Davis, ed., *Tensile testing*, 2nd edn., ASM International, United state of America, 2004.
44. J. H. Lee, Y. K. Jang, C. E. Hong, N. H. Kim, P. Li and H. K. Lee, *J. Power Sources*, 2009, **193**, 523-529.
45. P. Ramesh and S. Sampath, *Anal. Chem.*, 2003, **75**, 6949-6957.
46. T. Ndlovu, O. A. Arotiba, S. Sampath, R. W. Krause and B. B. Mamba, *Int. J. Electrochem. Sci.*, 2012, **7**, 9441-9453.
47. Y. H. Wen, H. M. Zhang, P. Qian, H. T. Zhou, P. Zhao, B. L. Yi and Y. S. Yang, *J. Electrochem. Soc.*, 2006, **153**, A929-A934.
48. M. Polzler, A. H. Whitehead and B. Gollas, *ECS Trans.*, 2010, **25**, 43-55.
49. G. Trejo, R. Ortega B., Y. Meas, P. Ozil, E. Chainet and B. Nguyen, *J. Electrochem. Soc.*, 1998, **145**, 4090-4097.
50. G. Trejo, H. Ruiz, R. O. Borges and Y. Meas, *J. Appl. Electrochem.*, 2001, **31**, 685-692.
51. Y. Hamlaoui, F. Pedraza, C. Remazeilles, S. Cohendoz, C. Rebere, L. Tifouti and J. Creus, *Mater. chem. phys.*, 2009, **113**, 650-657.
52. E. M. Geniès, A. Boyle, M. Lapkowski and C. Tsintavis, *Synth. Met.*, 1990, **36**, 139-182.
53. H. K. Hassan, N. F. Atta and A. Galal, *Int. J. Electrochem. Sci.*, 2012, **7**, 11161 - 11181.
54. S. E. Moulton, P. C. Innis, L. A. P. Kane-Maguire, O. Ngamna and G. G. Wallace, *Curr. Appl. Phys.*, 2004, **4**, 402-406.
55. A. K. Dutta, S. K. Maji, D. N. Srivastava, A. Mondal, P. Biswas, P. Paul and B. Adhikary, *J. Mol. Cata. A: Chem.*, 2012, **360**, 71-77.